A stochastic flow approach to model the mean velocity profile of wall-bounded flows

Benoît Pinier and Etienne Mémin

Inria/ IRMAR/ U. Rennes I, Campus universitaire de Beaulieu, 35042 Rennes Cedex, France

Sylvain Laizet

Department of Aeronautics, Imperial College London, South Kensington campus, London SW7 2AZ, UK

Roger Lewandowski

IRMAR/ U. Rennes I, Campus universitaire de Beaulieu, 35042 Rennes Cedex, France

(Dated: May 20, 2019)

Abstract

There is no satisfactory model to explain the mean velocity profile of the whole turbulent layer in canonical wall-bounded flows. In this paper, a mean velocity profile expression is proposed for wall-bounded turbulent flows based on a recently proposed stochastic representation of fluid flows dynamics. This original approach, called *modeling under location uncertainty* introduces in a rigorous way a subgrid term generalizing the eddy-viscosity assumption and an eddy-induced advection term resulting from turbulence inhomogeneity. This latter term gives rise to a theoretically well-grounded model for the transitional zone between the viscous sublayer and the turbulent sublayer. An expression of the small-scale velocity component is also provided in the viscous zone. Numerical assessments of the results are provided for turbulent boundary layer flows, pipe flows and channel flows at various Reynolds numbers.

I. INTRODUCTION

Mean velocity profiles in wall-bounded flows are an immense source of information for many industrial applications and in geophysics to model the interface between atmosphere and ocean. As a results, an intense research effort has been dedicated to their study. Since the seminal work of [1] and [2], the mean velocity profile is known to be linear in a viscous sublayer near the wall and logarithmic within a turbulent sublayer, located before a region of uniform mean profile. These assumptions have been derived from different theoretical arguments and confirmed in a wide variety of experiments [3–6]. For the interface between the viscous layer and the logarithmic layer, referred to as the buffer zone, no robust model is yet available.

The lack of a model with clear theoretical foundations for the buffer zone is essentially due to a change of the dynamical regime between the viscous and turbulent sublayers. In the former, the molecular friction dominates while in the latter it is a large-scale turbulent mixing dissipation which governs the flow. A transitional mechanism is necessarily acting in between these two regions. In this study it is shown that by taking properly into account the uncertainties associated with the unresolved (turbulent) components of wall-bounded flows, it is possible to introduce a theoretically well-defined model for the buffer zone. This model is directly associated to a statistical eddy-induced velocity. Such a drift correction corresponds to the so-called *turbophoresis* phenomenon associated with small-scale inhomogeneity, which drives inertial particles toward the regions of low turbulent diffusivity [7]. It is also akin to the velocity correction introduced for tracer mean transport in oceanic or atmospheric circulation models [8].

The new model used in this study is derived from a large-scale stochastic representation recently proposed by [9] and which has been applied with success for various turbulent flows [10–12]. The formulation, referred to as modeling under location uncertainty (LU), incorporates a random component as a model of the unresolved small-scale velocities. Its principles are briefly described in the below.

It is based on a decomposition of the Lagrangian velocity, with a large-scale smooth component, $\widetilde{\boldsymbol{u}}$, and an incompressible highly oscillating random component

$$\frac{\mathrm{d}\boldsymbol{X}_t}{\mathrm{d}t} = \widetilde{\boldsymbol{u}}(\boldsymbol{X}_t, t) + \boldsymbol{\sigma}(\boldsymbol{X}_t, t)\dot{\boldsymbol{B}}_t. \tag{1}$$

The first term represents the large-scale velocity component while the second one, written

(formally) as the time derivative of a d-dimentional Brownian function, $\dot{\boldsymbol{B}}_t = \mathrm{d}\boldsymbol{B}_t/\mathrm{d}t$, stands for the fast, unresolved, velocity component. The Brownian function, $\boldsymbol{B}_t$, is designed to have a unitary variance. It can be seen as a white noise in space and a Brownian function in time (formally it is $\mathbb{I}_d$-cylindrical Wiener process [13]). It is therefore assumed that the random velocity field is Gaussian and uncorrelated at the time scale of the large-scale velocity component. Such a random field leads to multiplicative nonGaussian noise when incorporated in transport equations. This stochastic formulation can be related to the Lagrangian stochastic models based on Langevin equations proposed for turbulent dispersion [14] or for probability density function (PDF) modelling of turbulent flows [15–17]. For the present work, this Lagrangian formulation is rather used to deduce the associated large-scale Eulerian representations of the flow dynamics.

The divergence-free random field involved in the Lagangian formulation (1) is defined over the fluid domain, Ω, through the kernel $\breve{\boldsymbol{\sigma}}(.,.,t)$ of the diffusion operator $\boldsymbol{\sigma}(.,t)$

$$\forall \boldsymbol{x} \in \Omega, \quad (\boldsymbol{\sigma}(\boldsymbol{x},t)\boldsymbol{f})^i \triangleq \sum_j \int_\Omega \breve{\sigma}^{ij}(\boldsymbol{x},\boldsymbol{y},t) f^j(\boldsymbol{y},t)\mathrm{d}\boldsymbol{y}, \ i,j = 1,\ldots,d. \tag{2}$$

This operator is assumed to be of finite norm. The covariance of the random turbulent component is defined as

$$Q_{ij}(\boldsymbol{x},\boldsymbol{x}',t,t') = \mathbb{E}\big((\boldsymbol{\sigma}(\boldsymbol{x},t)\mathrm{d}\boldsymbol{B}_t)_i(\boldsymbol{\sigma}(\boldsymbol{x}',t')\mathrm{d}\boldsymbol{B}_t)_j\big) = c_{ij}(\boldsymbol{x},\boldsymbol{x}',t)\delta(t-t')\mathrm{d}t,$$

and the diagonal of the covariance tensor, defined as $a_{ij}(\boldsymbol{x},t) = c_{ij}(\boldsymbol{x},\boldsymbol{x},t)$ is of crucial importance in the following. It has the dimension of diffusion (m^2/s) and plays the role of a *generalized* matrix-valued eddy viscosity. For canonical wall-bounded flows, it will be seen that only vertical variance coefficient a_{zz} is of particular interest. Otherwise, it is important to note that for isotropic random field the diffusion tensor depends only on the distance between two points. The variance tensor is consequently constant in that case. For divergence-free isotropic noise it is also diagonal [9] .

The rate of change of a scalar quantity q within a volume transported by the random flow (1) can be seen as a stochastic representation of the Reynolds transport theorem (RTT) [9]. For a divergence free random component the RTT reads

$$\mathrm{d}\int_{V(t)} q\mathrm{d}\boldsymbol{x} = \int_{V(t)} \big(\mathrm{d}_t q + \boldsymbol{\nabla}\cdot(q\widetilde{\boldsymbol{u}}^*)\mathrm{d}t + \boldsymbol{\sigma}\mathrm{d}\boldsymbol{B}_t\cdot\boldsymbol{\nabla}q - \boldsymbol{\nabla}\cdot(\frac{1}{2}\boldsymbol{a}\boldsymbol{\nabla}q)\big)\mathrm{d}t\mathrm{d}\boldsymbol{x}, \tag{3}$$

where the first term represents the increment in time of the random scalar q, and the effective advection velocity in the second term is defined as

$$\widetilde{\boldsymbol{u}}^* = \widetilde{\boldsymbol{u}} - \frac{1}{2}\boldsymbol{\nabla}\cdot\boldsymbol{a}. \tag{4}$$

From this expression the evolution of a conserved scalar (with an extensive property) reads immediately

$$\mathrm{d}_t q + \boldsymbol{\nabla}\cdot(q\widetilde{\boldsymbol{u}}^*)\mathrm{d}t + \boldsymbol{\sigma}\mathrm{d}\boldsymbol{B}_t\cdot\boldsymbol{\nabla}q - \boldsymbol{\nabla}\cdot(\frac{1}{2}\boldsymbol{a}\boldsymbol{\nabla}q)\mathrm{d}t = 0, \tag{5}$$

where the first term denotes a time increment of the scalar at a fixed position. This stochastic partial differential equation encompasses meaningful terms for turbulence study at large scale. As a matter of fact, the forth term is a dissipation term (with suitable boundary conditions)

$$\int_\Omega q\boldsymbol{\nabla}\cdot(\boldsymbol{a}\boldsymbol{\nabla}q)\mathrm{d}\boldsymbol{x} = -\int_\Omega \boldsymbol{\nabla}q^T\boldsymbol{a}\boldsymbol{\nabla}q\mathrm{d}\boldsymbol{x},$$

where the variance tensor, $\boldsymbol{a}$, is semi-definite positive. It includes the mixing mechanism due to the unresolved scales action. The third term represents the advection of the scalar quantity by the random velocity component. It can be noted that this term is multiplicative and therefore nonGaussian. The modified advection involved in the second term captures the action of the random field inhomogeneity on the transported scalar.

Incompressibility conditions for a fluid with a constant density are readily derived from (5) as

$$\boldsymbol{\nabla}\cdot\boldsymbol{\sigma}\mathrm{d}\boldsymbol{B}_t = 0, \tag{6a}$$

$$\boldsymbol{\nabla}\cdot\widetilde{\boldsymbol{u}}^* = \boldsymbol{\nabla}\cdot(\widetilde{\boldsymbol{u}} - \frac{1}{2}\boldsymbol{\nabla}\cdot\boldsymbol{a}) = 0. \tag{6b}$$

The first condition is intuitive and enforces a divergence-free random component, whereas the second constraint imposes a divergence-free condition on the effective advection. This last relation provides a link between the smooth resolved velocity component and the variance tensor divergence. For homogeneous random fields (such as isotropic turbulence) this equation can be reduced to a classic divergence-free condition on the resolved velocity component (as the variance tensor would be constant). For isochoric flows with variable density as in geophysical fluid dynamics, interested readers may have a look at [18–20]. An application of this framework to derive a stochastic representation of the Lorenz system is also described and studied in [21].

For incompressible flows, the stochastic transport equation (3) has the remarkable property to conserve the energy

$$\mathrm{d}\int_\Omega \frac{1}{2}q^2\mathrm{d}\boldsymbol{x} = -\int_\Omega \frac{1}{2}(\widetilde{\boldsymbol{u}}^*\mathrm{d}t+\boldsymbol{\sigma}\mathrm{d}\boldsymbol{B}_t)\cdot\boldsymbol{\nabla}q\mathrm{d}\boldsymbol{x}+\underbrace{\mathrm{d}t\int_\Omega q\boldsymbol{\nabla}\cdot(\boldsymbol{a}\boldsymbol{\nabla}q)\mathrm{d}\boldsymbol{x}}_{\text{Energy loss by diffusion}}+\underbrace{\mathrm{d}t\int_\Omega \boldsymbol{\nabla}q^T\boldsymbol{a}\boldsymbol{\nabla}q\mathrm{d}\boldsymbol{x}}_{\text{Energy intake by the noise}}=0.$$

The last term comes from Ito integration by part lemma. Equation (3) conserves thus the main specificity of a transport equation.

This stochastic RTT allows the derivation from the Newton second principle of the modified Navier-Stokes system of equations for an incompressible fluid [9, 18]

Momentum equations

$$\partial_t\widetilde{\boldsymbol{u}} + (\widetilde{\boldsymbol{u}}^*\cdot\boldsymbol{\nabla})\widetilde{\boldsymbol{u}} - \frac{1}{2}\boldsymbol{\nabla}\cdot\boldsymbol{\tau} = -\frac{1}{\rho}\boldsymbol{\nabla}p + \nu\boldsymbol{\nabla}^2\widetilde{\boldsymbol{u}}, \tag{7a}$$

Modified advection (turbophoresis)

$$\widetilde{\boldsymbol{u}}^* = \widetilde{\boldsymbol{u}} - \frac{1}{2}(\boldsymbol{\nabla}\cdot\boldsymbol{a}) \tag{7b}$$

Diffusion (subgrid tensor)

$$\boldsymbol{\tau} = (\boldsymbol{a}\boldsymbol{\nabla})\widetilde{\boldsymbol{u}} \tag{7c}$$

Pressure random contribution

$$\boldsymbol{\nabla}\mathrm{d}p_t = -\rho(\boldsymbol{\sigma}\mathrm{d}\hat{\boldsymbol{B}}_t\cdot\boldsymbol{\nabla})\widetilde{\boldsymbol{u}} + \nu\boldsymbol{\nabla}^2\boldsymbol{\sigma}\mathrm{d}\boldsymbol{B}_t, \tag{7d}$$

Mass conservation

$$\boldsymbol{\nabla}\cdot(\boldsymbol{\sigma}\mathrm{d}\boldsymbol{B}_t) = 0, \quad \boldsymbol{\nabla}\cdot\widetilde{\boldsymbol{u}} - \frac{1}{2}\boldsymbol{\nabla}\cdot(\boldsymbol{\nabla}\cdot\boldsymbol{a}) = 0. \tag{7e}$$

This system corresponds to a large-scale description of the flow in which the effect of the unresolved random turbulent component is explicitly taken into account. The scale separation in this system is obtained under the assumption of a smooth in time large scale component, well suited to the context of this study. A similar stochastic framework arising from an Hamiltonian principle has been proposed in [22] and analysed in [23] and [24]. This framework leads to enstrophy conservation whereas the LU formulation conserves the energy of a transported scalar [18].

A quite intuitive representation results from this formulation which includes a generalized (matrix valued) eddy-viscosity subgrid model, $(\boldsymbol{a}\boldsymbol{\nabla})\widetilde{\boldsymbol{u}}$, together with a correction of the advection term associated with turbulence inhomogeneity $(\boldsymbol{\nabla}\cdot\boldsymbol{a})$. These two terms depend

on the variance tensor, $\boldsymbol{a}(\boldsymbol{x})$. As mentioned previously, the modified advection describes the statistical effect caused by the inhomogeneity of the unresolved velocity component on the large scales. This term has the same form as the so-called turbophoresis term proposed in [7, 25, 26] to describe the drift of inertial particles toward regions of lower diffusivity in turbulent flow. It will be shown that this component plays a fundamental role in the transitional zone of wall-bounded flows. The term $\mathrm{d}p_t$ corresponds to the pressure associated with the random turbulent component, p is the large scale pressure, ρ is the density and ν the kinematic viscosity. The last constraint is a result of the mass conservation and imposes a divergence-free effective advection.

Compared to the traditional Reynolds decomposition, this decomposition does not rely on the time differentiability assumption of the velocity fluctuations. Assuming a random nature for these fluctuations and employing stochastic calculus rules to deal with them, it has the great advantage to let arise in a natural way several useful terms related to backscaterring (through the multiplicative noise), large-scale dissipation (via a diffusion term) and turbophoresis effect (associated with the modified advection). The presence or not of the first term, results from a scale separation principle between the random fluctuation and the large-scale component. With no scale separation, one get a stochastic partial differential equation for the momentum, whereas, a deterministic large-scale expression of the Navier-Stokes can be obtained through a theoretically justified scale separation associated with a temporal regularity assumption (formally a finite variation assumption) on the large-scale component (as it is the case in the present study). The shape of the dissipation operator has the great advantage to be known and, as a result, there is no need to invoke the Boussinesq assumption to model the Reynolds tensor. Furthermore, it should be noted that particular forms of the variance tensor lead to models that are similar to well-established models such as the Smagorinsky models [10, 11] or the Gent-McWilliams model for oceanic applications [9].

Note that though it is possible to describe accurately the large-scale evolution equation with the present approach, it is not possible to extract a dynamics for the unresolved components as they are uncorrelated in time. In the following, it will be seen that such an approach can lead to an accurate modeling of the mean velocity profile for wall-bounded flows.

In the next section, the ideal flow conditions pertaining to the classic derivation of the

mean velocity profile for wall-bounded flows is recalled and its expression for the model under location uncertainty is explained. In the following, the x direction is the streamwise direction, y the spanwise direction and z the wall normal direction.

II. BOUNDARY LAYER AND WALL LAWS

The derivation of the wall laws relies on the following hypothesis: the large-scale component $\widetilde{\boldsymbol{u}}$ is parallel to the wall plane $\{z = 0\}$ and depends only on the distance to the wall, z; the large-scale and small-scale velocity components are stationary and at the wall the flow velocity is zero ($\widetilde{\boldsymbol{u}} = 0$ and $\boldsymbol{\sigma} = 0$); the large-scale pressure p is constant.

The tangential cumulated friction per time interval, Δt, applied by the flow on the wall is expressed from the shear stress at the wall, which according to our model involves a large-scale component and a small-scale random component

$$S_t = \rho\nu \int_t^{t+\Delta t} \Big(\frac{\partial \widetilde{\boldsymbol{u}}}{\partial n}\mathrm{d}t + \frac{\partial \boldsymbol{\sigma}}{\partial n}\mathrm{d}\boldsymbol{B}_t\Big)\Big|_{z=0}. \tag{8}$$

The small-scale shear stress random field is assumed to be homogeneous with a constant variance tensor, $\boldsymbol{a}_n$ (dimension $[T]^{-1}$). This assumption, with no particular dependence on the horizontal plane of the shear stress variance is perfectly acceptable.

Invoking that the expectation $\mathbb{E}\|\int \boldsymbol{\sigma}\mathrm{d}\boldsymbol{B}_t\|^2 = \int tr\boldsymbol{a}\ \mathrm{d}t$ (Ito isometry) for the Brownian term in the previous equation (with tr defined as the matrix trace), it is possible to define the mean cumulated friction magnitude as

$$\mathbb{E}\|\boldsymbol{S}_t\|^2 = (\rho\nu)^2\Delta t \int |\partial_n \widetilde{\boldsymbol{u}}|^2\mathrm{d}t + (\rho\nu)^2 \int tr\boldsymbol{a}_n\mathrm{d}t. \tag{9}$$

Assuming the velocity $\partial_n\widetilde{\boldsymbol{u}}$ is constant, and since $\boldsymbol{a}_n$ is also constant

$$(\mathbb{E}\|\boldsymbol{S}_t\|^2)^{\frac{1}{2}} = (\rho\nu)\big(|\partial_n\widetilde{\boldsymbol{u}}|^2(\Delta t)^2 + \epsilon^2\Delta t\big)^{1/2} \tag{10}$$

where $\epsilon^2 = tr\boldsymbol{a}_n$ is defined as the variance of the small-scale shear stress.

The friction velocity $U_\tau\boldsymbol{\delta}\widetilde{\boldsymbol{u}}$ in the streamwise direction, $\boldsymbol{\delta}\widetilde{\boldsymbol{u}}$, is now defined from the shear stress as

$$U_\tau = \left(\frac{\mathbb{E}(\|S\|^2)^{1/2}}{\rho\Delta t}\right)^{1/2} = \left[\nu\left(|\partial_n\widetilde{\boldsymbol{u}}|^2 + \frac{1}{\Delta t}\epsilon^2\right)^{1/2}\right]^{1/2}. \tag{11}$$

This quantity scales as a velocity ($\sim (L^2/T^2)^{1/2}$) and for a null uncertainty $\epsilon^2 = 0$, the usual definition of the friction velocity is recovered, with $\widetilde{U}_\tau = (\nu|\partial_n\widetilde{\boldsymbol{u}}|)^{1/2}$). For a non null

uncertainty, a modified expression with a deviation from the standard definition depending on Δt can be derived. It is immediate to observe that when $\Delta t \to \infty$, $U_\tau \to \widetilde{U}_\tau$. However, for small time interval and large small-scale velocity stress at the wall, the deviation from the standard definition can be important. The friction velocity $U_\tau \approx \widetilde{U}_\tau$ is recovered only when the shear stress variance is much smaller than the time interval: $\epsilon^2 \ll \Delta t$. The usual friction velocity can be either computed from long-time (stationary) average velocity field (if available) or through (11) from smooth velocity snapshots and an estimation of the small-scale shear stress variance. This latter term plays the role of a correction that must be brought to the friction velocity computed from averages over a given time period, Δt, to obtain the mean. This case corresponds to the situation often encountered in studies of oceanic or atmospheric flows. Let us note that only the averaged friction velocity, $\widetilde{U}_\tau$, is required to obtain the mean velocity profile.

A. Boundary layer structure

It is well-established that the boundary layer is formed of two main sublayers: the viscous sublayer and the turbulent layer. The former corresponds to a region of contact between the wall and the fluid, where the flow is driven mainly by the molecular shear stress. In the latter, the flow is dominated by the large-scale shear stress associated with the unresolved fluctuations (here the small-scale random field). For the LU flow dynamics and the TBL ideal configuration described above, the stationary equations for the mean velocity component in these two sub-layers are described below.

1. Viscous sublayer

In the viscous sublayer, extending from the wall ($z = 0$) to a distance ($z = z_0$), molecular viscosity dominates the flow at all scales. From the proposed system (7), it can be seen that the large-scale drift component exhibits a constant variation with respect to depth, while the small-scale component is spatially very smooth (harmonic). The random turbulent pressure

diffusion term is consequently constant. To summarize,

Large-scale component

$$\nu\boldsymbol{\nabla}^2\widetilde{\boldsymbol{u}} = 0 \Rightarrow \partial_z\widetilde{\boldsymbol{u}} = C_1, \tag{12a}$$

Small scale component

$$\nu\boldsymbol{\nabla}^2\boldsymbol{\sigma}\mathrm{d}\boldsymbol{B}_t = 0 \Rightarrow \boldsymbol{\nabla}^2\boldsymbol{\sigma}^{ij} = 0, \tag{12b}$$

Turbulent pressure

$$\mathrm{d}p_t = C_2, \tag{12c}$$

Incompressibility

$$\boldsymbol{\nabla}\cdot(\boldsymbol{\sigma}\mathrm{d}\boldsymbol{B}_t) = 0. \tag{12d}$$

2. Turbulent sublayer

In the turbulent sublayer, delimited between the end of the viscous layer $z = z_0$ and an upper limit $z = z_1$, the dynamics is driven by the combination of the large-scale diffusion and the molecular friction. From the ideal TBL assumptions, the proposed system (7) reads

Large-scale component

$$-\partial_z a_{zz}\partial_z\widetilde{\boldsymbol{u}} - \partial_z\big((a_{zz} + 2\nu)\partial_z\widetilde{\boldsymbol{u}}\big) = 0, \tag{13a}$$

Turbulent pressure horizontal gradients

$$\boldsymbol{\nabla}_H\mathrm{d}p_t = \partial_z\widetilde{\boldsymbol{u}}(\boldsymbol{\sigma}\mathrm{d}\boldsymbol{B}_t)_z + \nu\boldsymbol{\nabla}^2(\boldsymbol{\sigma}\mathrm{d}\boldsymbol{B}_t)_H = 0, \tag{13b}$$

Turbulent pressure vertical gradient

$$\partial_z\mathrm{d}p_t = \nu\boldsymbol{\nabla}^2(\boldsymbol{\sigma}\mathrm{d}\boldsymbol{B}_t)_z, \tag{13c}$$

Incompressibility

$$\boldsymbol{\nabla}\cdot(\boldsymbol{\sigma}\mathrm{d}\boldsymbol{B}_t) = 0, \quad \boldsymbol{\nabla}\cdot(\boldsymbol{\nabla}\cdot\boldsymbol{a}) = 0. \tag{13d}$$

It can be seen that the modified advection term caused by an eventual inhomogeneity of the random velocity fluctuations appears in the first term of (13a). This contribution depends on the vertical variance coefficient, a_{zz}, of the variance tensor. The second term of this equation represents the diffusion due to both molecular friction and small-scale mixing effect. It also depends mainly on the vertical variance coefficient.

Within this framework, the expressions of the mean velocity profile can be inferred for both regions.

B. Velocity expression in the viscous sublayer

At the interface between the viscous and turbulent sublayers ($z = z_0$), because the large-scale normal derivative of the velocity is constant, a null advection of $\widetilde{\boldsymbol{u}}$ by the random field ($\partial_z \widetilde{\boldsymbol{u}}(\boldsymbol{\sigma}\mathrm{d}\boldsymbol{B}_t)_z = 0$) in the turbulent pressure equation (12c) implies that $(\boldsymbol{\sigma}\mathrm{d}\boldsymbol{B}_t)_z|_{z=z_0} = 0$. The null boundary condition of the random field at the wall and the harmonic condition (12b) together with the strong maximum principle indicates that the turbulent component is necessarily a 2D (*i.e.*$(\boldsymbol{\sigma}\mathrm{d}\boldsymbol{B}_t)_z = 0$) incompressible (12d) flow everywhere in the viscous layer. Note this 2D divergence-free random flow is not constant in the viscous sublayer volume as its horizontal components depends on depth. Integrating over the viscous layer depth the harmonic condition (12b) of this horizontal random field ($\boldsymbol{\nabla}_H^2(\boldsymbol{\sigma}\mathrm{d}\boldsymbol{B}_t)_H = -\partial_{zz}^2(\boldsymbol{\sigma}\mathrm{d}\boldsymbol{B}_t)_H$) (with the subscript H denoting the horizontal components) yields

$$\boldsymbol{\nabla}_H^2 \int_0^{z_0} (\boldsymbol{\sigma}\mathrm{d}\boldsymbol{B}_t)_H = -\,\partial_z(\boldsymbol{\sigma}\mathrm{d}\boldsymbol{B}_t)_H|_{z=z_0} + (\partial_n \boldsymbol{\sigma}\boldsymbol{B}_t)_H.$$

The left-hand side term corresponds to an empirical mean along the vertical direction. Since it is a zero-mean random variable, it tends to zero (when discretizing the interval with enough points) and thus

$$\partial_z(\boldsymbol{\sigma}\mathrm{d}\boldsymbol{B}_t)_H|_{z=z_0} = (\partial_n \boldsymbol{\sigma}\boldsymbol{B}_t)_H.$$

The random shear term on the right-hand side of this expression is an homogeneous field with variance $\epsilon^2 \mathrm{d}t$. The left-hand side random field has thus the same characteristics. As a consequence, at fixed depth, the small-scale component $(\boldsymbol{\sigma}\mathrm{d}\boldsymbol{B}_t)_H$ is a homogeneous random field. Due to the harmonic constraint and the strong maximum principle, its diffusion tensor increases linearly with z. Therefore, the entire random field can be defined from a unitary 2D divergence-free Gaussian random field, $\boldsymbol{\eta}_t$, in the entire viscous layer as

$$(\boldsymbol{\sigma}(\boldsymbol{x})\mathrm{d}\boldsymbol{B}_t) = \epsilon z \sqrt{\mathrm{d}t}\, \boldsymbol{\eta}(\boldsymbol{x}),\ \forall z \in [0, z_0]. \tag{14}$$

It is therefore possible to state that in the viscous sublayer the small-scale component is a homogeneous 2D divergence-free random field with a variance that depends on the wall shear stress variance and growths as the square of the depth. Its vorticity is slanted, $\boldsymbol{\nabla} \times$

$\boldsymbol{\sigma}(\boldsymbol{x})\mathrm{d}\boldsymbol{B}_t = \epsilon\sqrt{\mathrm{d}t}(-\eta_y, \eta_x, z(\partial_x\eta_y - \partial_y\eta_x))^T$ and its mean magnitude intensifies linearly with the distance to the wall.

Besides, from the friction velocity definition (11), (12a) and because $\partial_z\widetilde{\boldsymbol{u}} = \partial_n\widetilde{\boldsymbol{u}} = C_1$ (with $\partial_z\widetilde{\boldsymbol{u}} > 0$)

$$\partial_z\widetilde{\boldsymbol{u}} = \big(\frac{1}{\nu^2}U_\tau^4 - \frac{1}{\Delta t}\epsilon^2\big)^{1/2}\boldsymbol{\delta}\widetilde{\boldsymbol{u}} = \frac{1}{\nu}\widetilde{U}_\tau^2\boldsymbol{\delta}\widetilde{\boldsymbol{u}}, \tag{15}$$

where $\widetilde{U}_\tau = (\nu|\partial_n\widetilde{\boldsymbol{u}}|)^{1/2}$ stands for the friction velocity associated with the large-scale component. Integrating along z and since $\widetilde{\boldsymbol{u}}(0) = 0$, the following expression for $\widetilde{\boldsymbol{u}}(z)$ can be obtained

$$\widetilde{\boldsymbol{u}}(z) = \frac{1}{\nu}\widetilde{U}_\tau^2 z\ \boldsymbol{\delta}\widetilde{\boldsymbol{u}}. \tag{16}$$

Gathering the large-scale and small-scale components, the entire infinitesimal displacement field over time interval, Δt, in the viscous layer finally reads

$$\forall z \in [0, z_0]\ \ \boldsymbol{u}(z)\Delta t = \frac{1}{\nu}\widetilde{U}_\tau^2 z\ \boldsymbol{\delta}\widetilde{\boldsymbol{u}}\Delta t + \epsilon z(\Delta t)^{1/2}\boldsymbol{\eta}. \tag{17}$$

The small-scale zero-mean random displacement has a variance $V = \epsilon^2 z^2\Delta t$. The variance tensor, $\boldsymbol{a} = \boldsymbol{\sigma}\boldsymbol{\sigma}^T$, is diagonal, depends only on z and scales as z^2. Because the small-scale random field is 2D, it should be noted that the vertical variance and cross-variance coefficients (namely a_{xz}, a_{yz}, and a_{zz}) are all null in the viscous layer. The mean velocity profile is given by (16) and the usual linear expression can be recovered. This linear profile is valid up to depth z_0, which is similar to the usual frictional length scale: $z_f = \nu/\widetilde{U}_\tau$. It is interesting to note that this profile can be specified from the friction velocity associated with the long-time average velocity field (if it can be computed), or from (11) if only smooth velocity snapshots on a given period of time together with an estimation of the small-scale shear stress variance are available. This latter case corresponds to the situation often encountered in studies of oceanic or atmospheric flows.

C. Velocity expression in the buffer and turbulent sublayer

In the vicinity of the viscous sublayer the molecular friction still dominates whereas at the end of the turbulent sublayer the large-scale shear stress is predominant and depends directly on the small-scale variance. Towards the end of the turbulent sublayer, it is reasonnable to assume that the variance tensor (i.e. the large-scale diffusion) dominates the molecular

viscosity. According to this hypothesis, an eddy-viscosity formulation can be obtained from (13a)

$$-\partial_z a_{zz} \partial_z \widetilde{\boldsymbol{u}} - \partial_z \big(a_{zz} \partial_z \widetilde{\boldsymbol{u}} \big) = 0. \tag{18}$$

It leads to the traditional logarithmic velocity profile when the first term is neglected and the eddy viscosity is assumed linear for the entire turbulent layer. This logarithmic profile provides a very good model, however it is known to poorly fit the transitional buffer region just after the viscous layer. For that reason, the turbulent layer is usually splitted into a logarithmic region and a transitional buffer zone.

1. Buffer zone

In the buffer zone, delimited by the end of the viscous layer, z_0, and the beginning of the logarithmic region, z_L, a strict independence of the variance tensor with respect to the horizontal directions can be assumed (continuity of the viscous zone). With this assumption, the small-scale component is a 3D homogeneous random field at a fixed depth. In other words, the variance tensor, $\boldsymbol{a}$, only depends on depth. It will be shown in the following that diverging from this hypothesis marks the beginning of the logarithmic zone (or equivalently the end of the buffer zone).

From the incompressibility constraint (13d), it can be written that

$$\boldsymbol{\nabla} \cdot \boldsymbol{\nabla} \cdot \boldsymbol{a} = 0 \implies \partial^2_{zz} a = 0 \implies \partial_z a_{zz} = C'. \tag{19}$$

At the interface $a_{zz}(z_0) = 0$, $a_{zz}(z) = C'(z - z_0)$ where C' scales as a velocity. To get an expression of the mean velocity profile with the same parameters as in the viscous layer, it is natural to express the vertical tensor variance in terms of the mean friction velocity

$$a_{zz}(z) = \widetilde{\kappa} \widetilde{U}_\tau (z - z_0), \tag{20}$$

with the constant $\widetilde{\kappa}$. This constant is related to the slope of the variance tensor coefficient along z. It is completely different from the von Kármán constant linked to the logarithmic region, even if it is defined with the same notation, to facilitate a connection with conventional wall law models.

At the interface $z = z_0$, and using (16)

$$\partial_z \widetilde{\boldsymbol{u}}(z_0) = \frac{1}{\nu} \widetilde{U}^2_\tau \boldsymbol{\delta} \widetilde{\boldsymbol{u}}, \tag{21}$$

and a null value for the vertical variance tensor ($a_{zz} = 0$). Integrating (13a) with boundary condition (21) gives an expression for $\partial_z \widetilde{\boldsymbol{u}}$. A second integration of the same equation yields the following velocity profile within the buffer zone

$$\forall z \in [z_0, z_L] \;\; \widetilde{\boldsymbol{u}}(z) = \widetilde{\boldsymbol{u}}(z_0) - \widetilde{U}_\tau \frac{4\nu}{\widetilde{\kappa}} \left(\frac{1}{\widetilde{\kappa}\widetilde{U}_\tau (z - z_0) + 2\nu} - \frac{1}{2\nu} \right) \delta\widetilde{\boldsymbol{u}}. \tag{22}$$

It can be checked that $\widetilde{\boldsymbol{u}}(z)$ and $\partial_z \widetilde{\boldsymbol{u}}(z)$ are indeed positive and therefore satisfy the fundamental properties of the large-scale velocity in a TBL. The buffer zone is restricted to an area located between the end of the viscous zone (at $z = z_0$) and the beginning of the logarithmic region (at $z = z_L$). The end of the viscous zone, z_0, and the constant $\widetilde{\kappa}$ are the only parameters of the velocity and variance tensor profiles in the buffer zone. The end of the buffer zone is characterized by a change of regime of the variance tensor profile. It is also characterized by a gradual loss of influence of the wall-normal component of the turbophoresis drift, while it is constant in the buffer zone ($\partial_z a_{zz} = \widetilde{\kappa}\widetilde{U}_\tau$).

2. Logarithmic region

Towards the end of the turbulent layer, the mean velocity profile can be described with a logarithmic shape. Several experiments and simulations have confirmed this shape from low to high Reynolds numbers. In the present framework, with a linear expression of the vertical variance coefficient it is not possible to reach such a logarithmic profile from two successive integrations of (18). This coefficient necessarily scales as the square-root of the wall distance ($a_{zz} \sim \sqrt{z}$). With that scaling and because the flow is continuous in the entire turbulent boundary layer, the following expression for the wall-normal variance tensor value can be obtained

$$a_{zz}(z) = \widetilde{\kappa}\widetilde{U}_\tau (z_L - z_0) \sqrt{\frac{z}{z_L}}, \;\; \forall z \in [z_L, z_1], \tag{23}$$

To satisfy the incompressibility condition (13d), such an expression comes to relax the strict independence on x and y of the variance tensor (i.e. $\partial^2_{z^2} a_{zz} \neq 0$). This is coherent with the occurence in the flow of elongated structures such as streaks (see [27] for a recent and complete review on the subject). In that sense the transition between the buffer region and the logarithmic layer can be seen as a change from homogeneous statistics at a fixed depth to an inhomogeneous distribution of the fluctuations with a dependency on the spanwise and streamwise coordinates.

With such a model for the variance tensor within the region located between the buffer zone limit (z_L) and the end of the turbulent sublayer (z_1), $\widetilde{\boldsymbol{u}}(z)$ can be expressed as

$$\widetilde{\boldsymbol{u}}(z) = \widetilde{\boldsymbol{u}}(z_L) + \partial_z \widetilde{\boldsymbol{u}}(z_L) z_L \ln\left(\frac{z}{z_L}\right). \tag{24}$$

This profile differs slightly from the usual logarithmic law. It is interesting to note that it takes the form of a general log-law for rough boundary, where z_L plays the role of the roughness length. The factor in front of the log-law is given through the buffer velocity profile as

$$z_L \partial_z \widetilde{\boldsymbol{u}}(z_L) = \frac{4\nu \widetilde{U}_\tau^2 z_L}{\left(\widetilde{\kappa}\widetilde{U}_\tau(z_L - z_0) + 2\nu\right)^2}. \tag{25}$$

In particular, the von Kármán constant, which weights the usual log-law, would here be defined as $\kappa = \widetilde{U}_\tau/(z_L \partial_z \widetilde{\boldsymbol{u}}(z_L))$. In the present study, it has a more complex expression which depends among other things on the separation limit between the buffer zone and the logarithmic region. In the logarithmic region the velocity and the variance tensor profile depend both on three parameters: z_0, z_L and $\widetilde{\kappa}$. These profiles are valid up to the limit of the turbulent boundary layer z_1. A scaling for z_L can be found by intersecting the logarithmic velocity profile and the linear velocity profile of the viscous zone. Neglecting the influence of the molecular viscosity in $\widetilde{\boldsymbol{u}}(z_L)$ and $z_L \partial_z \widetilde{\boldsymbol{u}}(z_L)$ yields $z_L \propto \frac{2}{\widetilde{\kappa}} z_f$.

It is important to stress that the modified logarithm velocity profile has been obtained from (18) neglecting the influence of the molecular viscosity in the momentum equation (13a). It is also possible to obtained a mean velocity profile for the logarithmic layer without neglecting the molecular viscosity (see appendix A). It is shown that the modified law obtained in (24) corresponds to a zero-order approximation in terms of the viscosity power.

D. Summary

The proposed stochastic flow model, built from a separation of the Lagrangian velocity in terms of smooth and random components, allows us to formalize a continuous model for the mean velocity profile within a turbulent layer of wall-bounded flows. Due to a proper modification of the advection velocity induced by the turbulence inhomogeneity and figuring the statistical effect of the small-scale velocity on the resolved components, the proposed new model enables to connect the two classic velocity profiles in the viscous and logarithmic sublayers. The velocity profile in this transitional so-called buffer zone scales as $1/z$. In

the viscous and logarithmic layers, as already observed from numerous experiments and classic flow models, the velocity profiles remains linear and logarithmic, respectively. The mean velocity profile, derived from the proposed stochastic uncertainty principle, depends on a matrix valued eddy viscosity function, called the variance tensor, and is related to the variance of the (random) velocity fluctuations. In the viscous layer, this variance tensor is 2D, diagonal and depends only on depth. The homogeneous nature of the random field at a fixed depth inherits from the homogeneous character of the random shear stress on the wall of the ideal wall-bounded flow configuration. Within the buffer zone, the random field is still homogeneous at a fixed depth but becomes tridimensional. The variance tensor coefficients still depend on the depth. The beginning of the logarithmic layer marks a break with this homogeneous character (at a fixed depth). The random field necessary depends on the steamwise and spanwise coordinates as well, making the model receptive to the emergence of inhomogeneous spatial structures such as streaks.

In the viscous and turbulent layers, the main parameter of the velocity profile (aside from the friction velocity) is the variance tensor coefficient in the wall normal direction, a_{zz}. This coefficient scales as $a_{zz} \propto 0$; $a_{zz} \propto z$; and as $a_{zz} \propto \sqrt{z}$ in the viscous, buffer and logarithmic zones, respectively. The full profile depends on the usual friction velocity defined either from the average velocity field, or from shorter-time averages and an estimation of the small-scale shear stress variance. It depends also on three parameters which are the depth of the viscous layer, the depth of the logarithmic zone start (or the end of the buffer sublayer) and a constant related to the slope of the wall-normal eddy viscosity a_{zz} in the buffer zone. As shown in the next section these parameters can easily be obtained from experimental or numerical flow data.

III. NUMERICAL VALIDATION

This section is dedicated to various numerical assessments of the theoretical expressions derived in the previous section with a particular focus on the mean velocity profiles for different wall-bounded flows at moderate to high Reynolds numbers. For completeness, the mean velocity profile for the three main type of wall-bounded flow will be studied (turbulent boundary layer flows, pipe flows or channel flows), using well-documented data from the literature.

The turbulent boundary layer simulations are provided by the Universidad Politecnica de Madrid and are described in [28–30]. These simulations lies in a range $\mathrm{Re}_\theta \in [2780 - 6650]$ and an equivalent Reynolds friction number $\mathrm{Re}_\tau \in [1000, 2000]$. The adimensional Reynold number $\mathrm{Re}_\theta = U_\infty \theta/\nu$ is based on the free-stream velocity U_∞ and the momentum thickness $\theta = \int_0^\infty U/U_\infty(1 - U/U_\infty)\mathrm{d}y$. The Reynolds friction number defined as $\mathrm{Re}_\tau = U_\tau \delta/\nu$ is based on the kinematic viscosity, the friction velocity, and the flow thickness δ, which is taken to be the half-width in channels, the 99% thickness in boundary layers, and the radius in pipes. The velocity profiles of the pipe flow simulations are provided by the Royal Institute of Technology of Stockolm (KTH), with data at $\mathrm{Re}_\tau = 180$, 360, 550, and 1000. These simulations are described and analyzed in [31]. As a last example, a channel flow is also considered for a very high Reynolds number case ($\mathrm{Re}_\tau \approx 5200$), using the simulation described in [32].

In the present study and for the three wall-bounded flows, the limit of the viscous zone (z_0), the constant $\widetilde{\kappa}$ and the limit of the buffer zone are estimated through a least-squares procedure and a gradient descent optimization. The least squares cost function between the data and the model is expressed on a section going from the wall to the end of the logarithmic section. The initial value of the parameter are manually fixed from a first rough profile. All the plots and results are provided in terms of the frictional length scale $z^+ = z\widetilde{U}_\tau/\nu$ and the friction velocity $u^+ = u/\widetilde{U}_\tau$. The parameter vector of the model $\hat{\Theta} = (z_0, z_L, \tilde{\kappa})^T$ is estimated through a least-squares fitting procedure with

$$\hat{\Theta} = \arg\min_{\Theta} \sum_i \|\boldsymbol{u}_\Theta(z_i) - \overline{\boldsymbol{u}}(z_i)\|^2.$$

This cost function between the parametric profile, $\boldsymbol{u}_\Theta$ and the flow velocities averaged in time and in the spanwise and streamwise directions, $\overline{\boldsymbol{u}}$, is minimized through a gradient descent procedure. The cost function support is roughly set to the height of the turbulent boundary layer. Note however that as the cost function is nonlinear in these parameters, the minimization is started from empirical values close enough to the sought values.

A. Turbulent boundary layer

The optimal triplet of parameters associated with the reconstructed mean velocity profiles is gathered in table I. It can be observed that the values of these parameters vary differently.

TABLE I. Parameters of the mean velocity profile for turbulent boundary layer flows.

Re_τ	z_0^+	z_L^+	$\widetilde{\kappa}$
1306	4.94	48.22	0.158
1437	4.97	48.29	0.157
1709	5.08	49.01	0.161
1989	4.90	50.38	0.158

The limit of the viscous zone lies in a tight range around $z_0^+ = 5$. The end of the buffer zone, in the other hand, varies more significantly when the Reynolds number is increased. The constant, $\widetilde{\kappa}$ (which corresponds to the slope of the variance tensor coefficient (along z) in the buffer zone), is almost constant and lies within a range between 0.157 and 0.161.

The profiles of the new model are compared to the classic wall laws: $\widetilde{\boldsymbol{u}} = z\widetilde{U}_\tau^2/\nu$ in the viscous sublayer, and $\widetilde{\boldsymbol{u}} = \widetilde{U}_\tau \left(\frac{1}{\kappa}\ln(z\frac{\widetilde{U}_\tau}{\nu}) + B\right)$ above the viscous sublayer, where the constants κ and B are optimally set from the data. The results are shown in figures 1–4 for $\mathrm{Re}_\tau = 1306$, 1437, 1709, and 1989 respectively.

In the viscous sublayer, there is no difference between the classic models and the new one (16). Both of them perfectly superimpose with the reference data. In that region, the variance tensor along the wall-normal direction, a_{zz}, is zero.

In the buffer region, where $a_{zz}(z)$ is linear, there is no theoretically well grounded model available for the velocity profile. In this transition area both the classic linear and logarithmic approximations deviate significantly from the reference profiles. On the other hand, the new model fits very nicely the data for the range of Reynolds number investigated in this study. The LU model, unlike adhoc formulation [33], enables us to devise a physically coherent model, in which a modified advection arising from the unresolved velocity inhomogeneity plays a fondamental role.

In the logarithmic region, both the classic log-law model and the LU model perform similarly and provide very good results for $\mathrm{Re}_\tau = 1306$ and 1437. For higher Reynolds numbers ($\mathrm{Re}_\tau = 1709$, and 1989) the agreement is equally good. Note however that the LU log profile is the best fit to the reference data. The good performance of the LU mean velocity profile supports the validity of the wall-normal variance tensor profile in the turbulent layer (e.g. linear and square-root profiles of $a_{zz}(z)$ in the buffer zone and in logarithmic layer

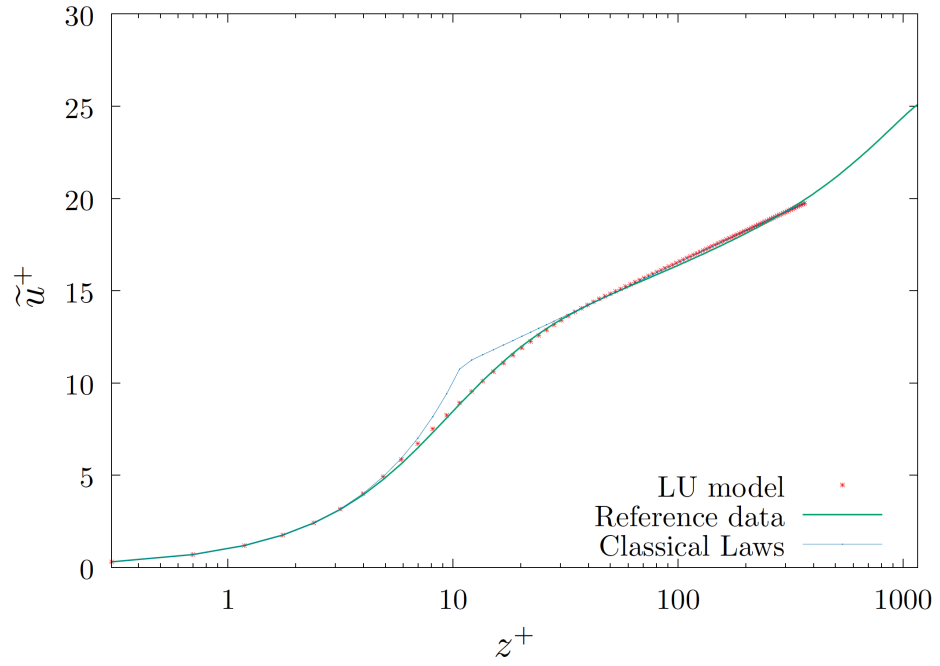

FIG. 1. Velocity profiles for the turbulent boundary layer at $\mathrm{Re}_\tau = 1306$. The green curve corresponds to the reference data. The blue dot lines show the classic laws (linear then logarithmic) and the red dots corresponds to the profile of the model under location uncertainty.

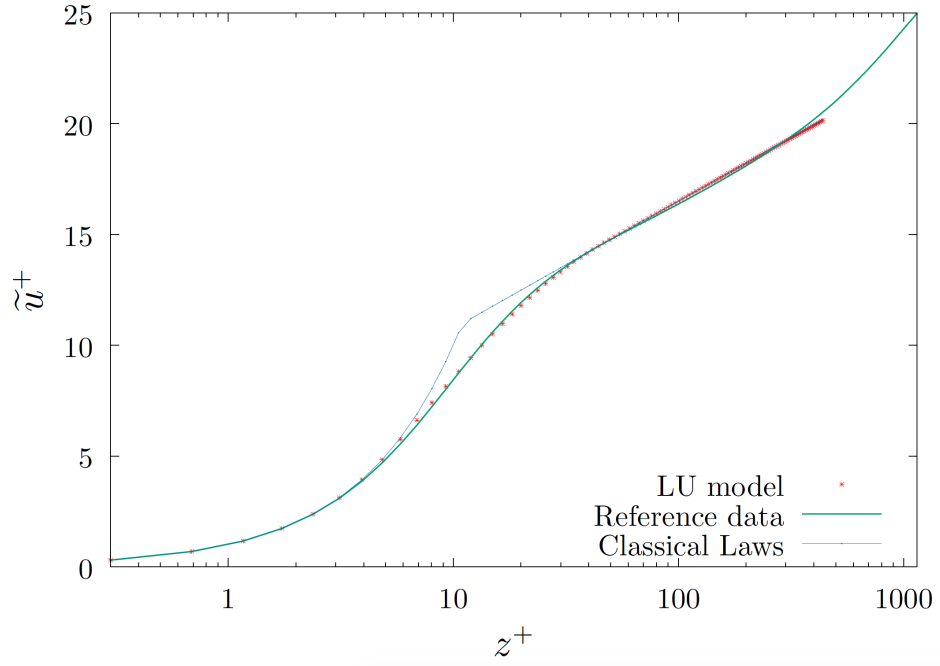

FIG. 2. Velocity profiles for the turbulent boundary layer at $\mathrm{Re}_\tau = 1437$. The green curve corresponds to the reference data. The blue dot lines show the classic laws (linear then logarithmic) and the red dots corresponds to the profile of the model under location uncertainty.

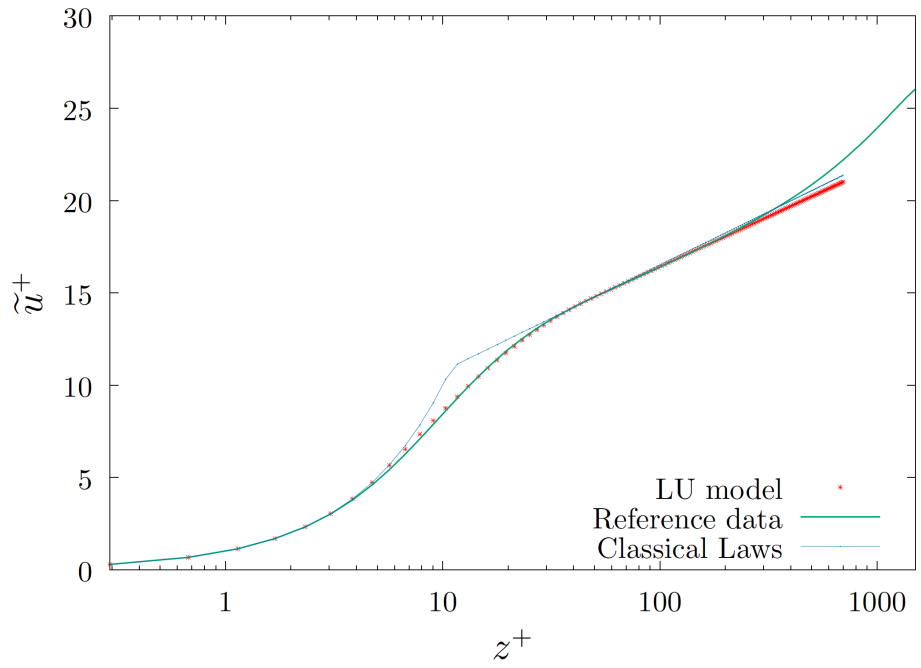

FIG. 3. Velocity profiles for the turbulent boundary layer at $\mathrm{Re}_\tau = 1709$. The green curve corresponds to the reference data. The blue dot lines show the classic laws (linear then logarithmic) and the red dots corresponds to the profile of the model under location uncertainty.

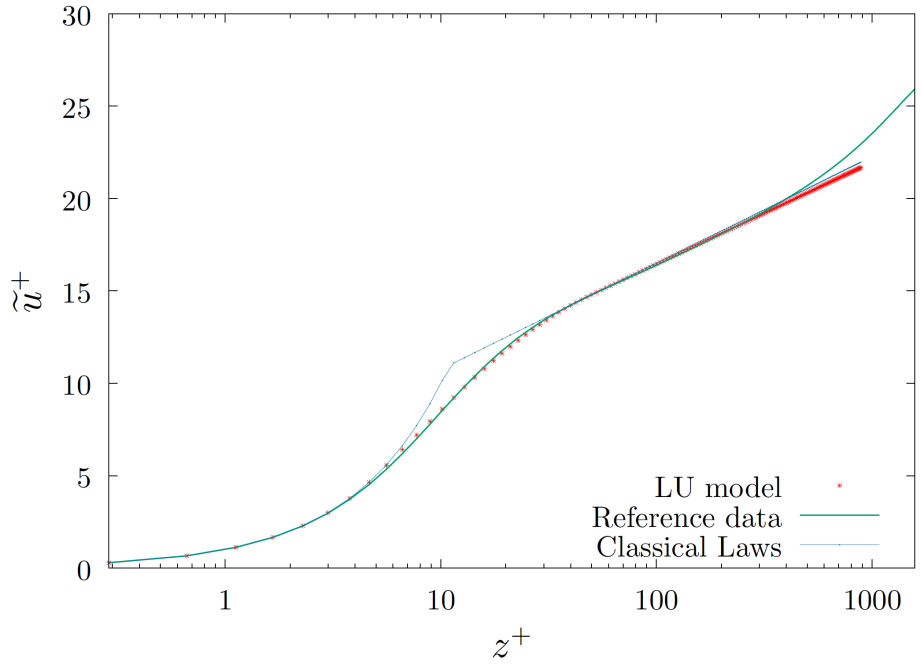

FIG. 4. Velocity profiles for the turbulent boundary layer at $\mathrm{Re}_\tau = 1989$. The green curve corresponds to the reference data. The blue dot lines show the classic laws (linear then logarithmic) and the red dots corresponds to the profile of the model under location uncertainty.

TABLE II. Parameters value of the mean velocity profile for pipe flows

Re_τ	z_0^+	z_L^+	$\widetilde{\kappa}$
180	5.61	43.75	0.150
360	5.27	43.85	0.158
550	5.11	46.31	0.158
1000	5.05	49.00	0.158

respectively) as the velocity profile highly depends on $\partial_z a_{zz} \partial_z \widetilde{\boldsymbol{u}}(z_l)$ (13a).

B. Pipe Flow

The optimal parameters are shown in table II. It can be seen that the value of the viscous layer thickness z_0^+ decreases with the increase of the friction Reynolds number, while the limit of the buffer zone z_L^+ grows; $\widetilde{\kappa}$ remains almost constant except for the first simulation associated with the lowest friction Reynolds number.

The mean velocity profiles are plotted in figures 5,6, 7, and 8. As for the turbulent boundary layer data, the modified LU model is shown in red, and is compared with the reference data and the classic logarithmic and viscous velocity profiles. Note that when compared to turbulent boundary layer flows, pipe flows exhibits a much shorter logarithmic layer. Similarly to the turbulent boundary layer, it can be seen that the proposed model is almost in perfect agreement with the data up to the end of the logarithmic layer. This model is again particularly relevant for the buffer zone, where no physical model has yet been derived in the literature from a classic eddy-viscosity concept.

C. Channel flow

For completeness, the mean velocity profile in a channel flow at $\mathrm{Re}_\tau = 5200$ is investigated using the data of [32]. For this flow, the parameters estimated from the data are gathered in table III. As it can be observed, the parameters are sensibly the same as in the previous examples, but with a shorter buffer region. The mean velocity profiles are shown in figure 9. As previously, the LU model can match very well the reference data. In the buffer zone

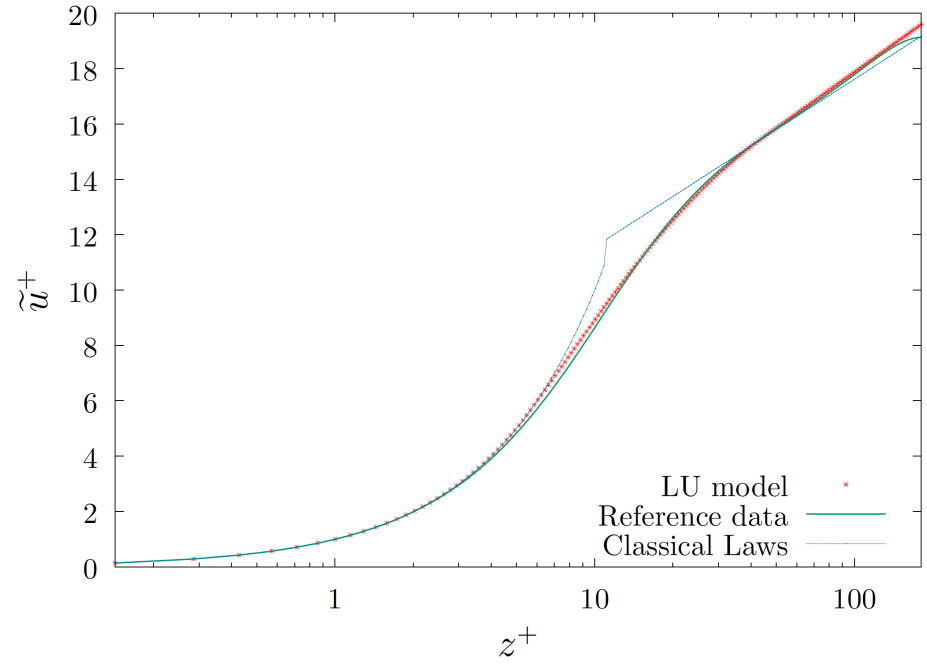

FIG. 5. Velocity profiles for the pipe flow at $\mathrm{Re}_\tau = 180$. The green curve corresponds to the reference data. The blue dot lines show the classic laws (linear then logarithmic) and the red dots corresponds to the profile of the model under location uncertainty.

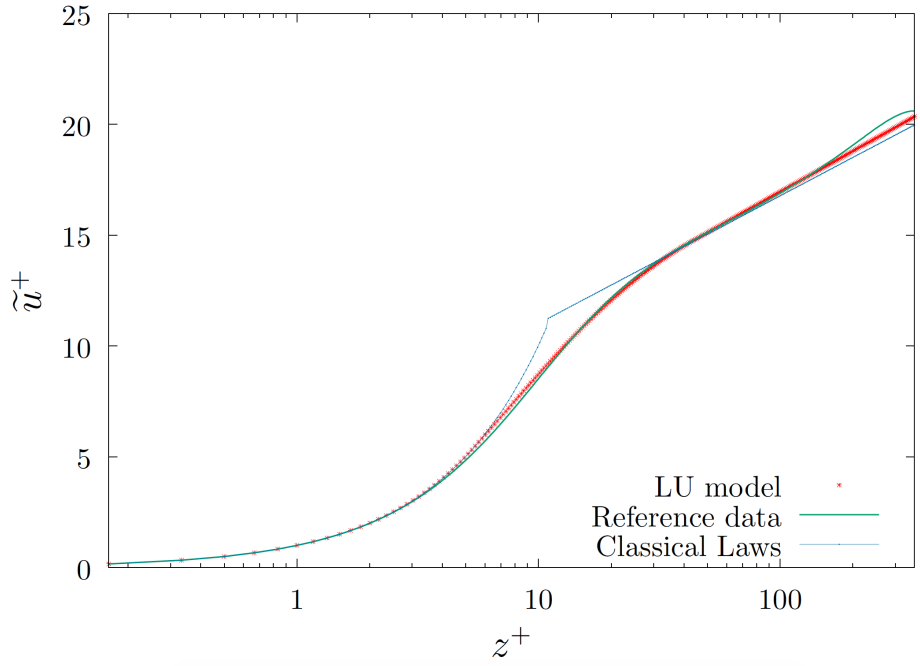

FIG. 6. Velocity profiles for the pipe flow at $\mathrm{Re}_\tau = 360$. The green curve corresponds to the reference data. The blue dot lines show the classic laws (linear then logarithmic) and the red dots corresponds to the profile of the model under location uncertainty.

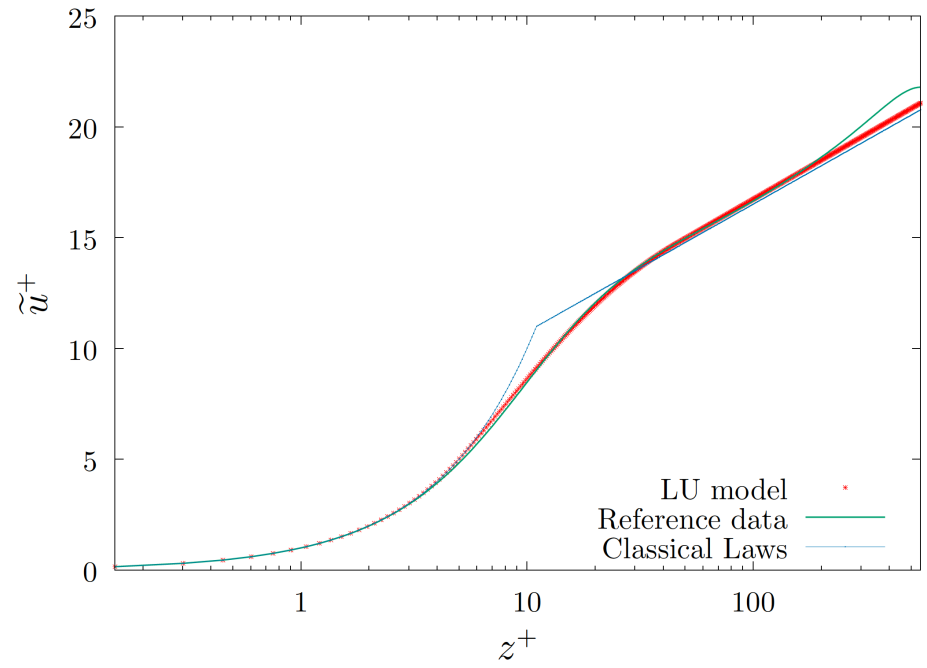

FIG. 7. Velocity profiles for the pipe flow at $\mathrm{Re}_\tau = 550$. The green curve corresponds to the reference data. The blue dot lines show the classic laws (linear then logarithmic) and the red dots corresponds to the profile of the model under location uncertainty.

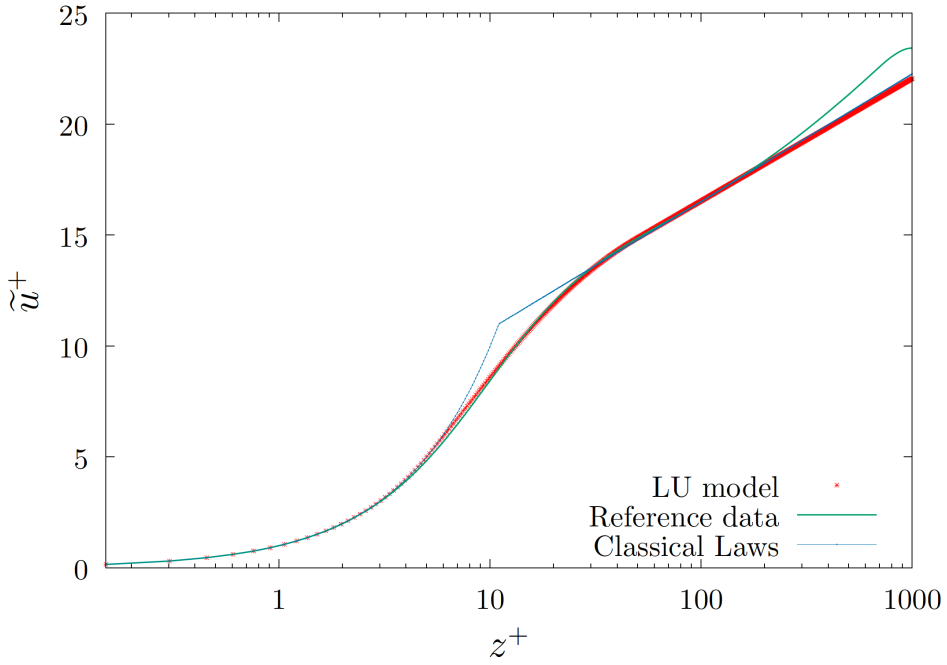

FIG. 8. Velocity profiles for the pipe flow at $\mathrm{Re}_\tau = 1000$. The green curve corresponds to the reference data. The blue dot lines show the classic laws (linear then logarithmic) and the red dots corresponds to the profile of the model under location uncertainty.

TABLE III. Parameters value of the mean velocity profile for a channel flow

Re_τ	z_0^+	z_L^+	$\widetilde{\kappa}$
5200	5.0	45.0	0.16

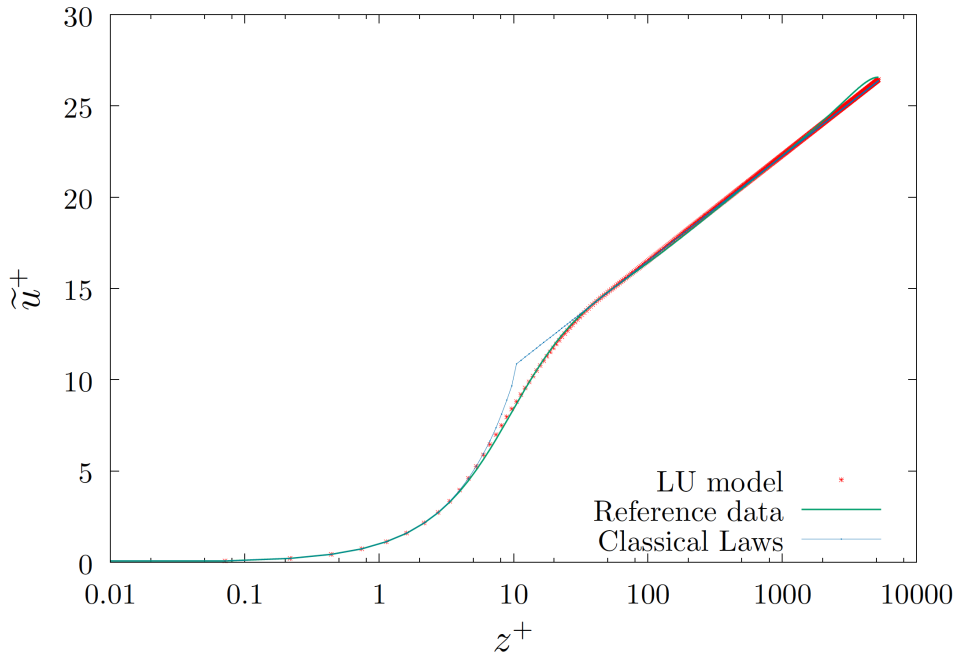

FIG. 9. Mean velocity profiles for the channel flow at $\mathrm{Re}_\tau \approx 5200$ [32]. The green curve corresponds to the reference data. The blue dot lines show the classic laws (linear then logarithmic) and the red dots corresponds to the profile of the model under location uncertainty.

the LU model almost perfectly fit the data. In the logarithmic region the LU logarithmic law and the classic one perform identically.

IV. CONCLUSION

The modeling under location uncertainty provides a novel expression for the mean velocity profile in wall-bounded turbulent flows. Using numerical data from three different types of wall-bounded flows, going from moderate to high Reynolds numbers, it is shown that the LU model allows us to devise a physical model for the mean velocity profile that matches very well the reference data for the full turbulent boundary layer while remaining continuous and differentiable. The derivation unveils in particular the role played by the advection

correction due to turbulence inhomogeneity in the transitional zone between the viscous and the logarithmic sublayers. This model is very promising as it provides for the first time (to the best of our knowledge) a physically relevant model for the buffer region. The LU derivation relies on a random modeling of the fluctuation velocity fields and exhibits a tensor playing the role of a matrix valued eddy-viscosity term generalizing de facto the Boussinesq assumption and the Prandlt mixing length. This tensor corresponds to the fluctuation variance multiplied by a decorrelation time; its wall-normal component is null in the viscous zone, linear in the buffer zone and scales as $\sqrt{z^+}$ in the logarithmic layer. The inhomogeneity of this tensor enforces a modified advection term which can be interpreted as the statistical influence of the fluctuation inhomogeneity on the large-scale advection component. This modification has a major contribution in the transitional buffer zone. The new velocity profile associated with the LU model relies on a new parameter linked to the slope of the variance tensor wall-normal component in the buffer zone and on the limits of the buffer zone. Based on the reference data used in the present study, the mean value of $\widetilde{\kappa}$ is 0.158, with a standard deviation of 0.003. According to the literature, the value of the well-known von Kármán constant is 0.4 ± 0.01 [34]. The limit of the viscous zone has the usual scaling of the frictional length $z_0 \propto z_f = \nu/\widetilde{U}_\tau$, while the end of the buffer zone scales as $z_L^+ \propto 2/\widetilde{\kappa}$, which, according to the mean value of the constant, gives $z_L^+ \propto 12.7$.

This new model opens very exciting perspectives for the set up of models "à la" Monin-Obukhov for fluid flows with thermal stratification as well as the establishment of more accurate wall functions for Large Eddy Simulations. It can also be a very useful tool for industrial problems involving pipe flows.

Appendix A: Generalized mean velocity profile in the logarithmic region

This appendix is dedicated to the derivation of a general mean velocity profile for the logarithmic layer without neglecting the molecular viscosity. It is shown that the modified law obtained in (24) corresponds to a zero order approximation in terms of the viscosity power.

The aim is to find a solution of

$$2\partial_z a_{zz} \partial_z \widetilde{\boldsymbol{u}} = -(a_{zz} + 2\nu)\partial_{zz}^2 \widetilde{\boldsymbol{u}}, \quad \forall z \in [z_L, z_1], \tag{A1}$$

with $a_{zz} = \widetilde{\kappa}\widetilde{U}_\tau(z_L - z_0)\sqrt{\frac{z}{z_L}}$ and where $a(z_L)$ and $\widetilde{\boldsymbol{u}}(z_L)$ are given by the profiles in the buffer region. In the following, the subscript of a_{zz} is dropped for clarity. Integrating (A1) between z_L and z

$$-2\int_{z_L}^{z}\frac{\partial_z a}{a+2\nu}\mathrm{d}z = \int_{z_L}^{z}\frac{\partial^2_{zz}\widetilde{\boldsymbol{u}}}{\partial_z\widetilde{\boldsymbol{u}}},$$

gives

$$2\log(a(z)+2\nu) - 2\log(a(z_L)+2\nu) = \log\frac{\partial_z\widetilde{\boldsymbol{u}}}{\partial_z\widetilde{\boldsymbol{u}}(z_L)}.$$

Linearizing to first order the log terms around $a(z)$ and $a(z_L)$

$$\log\big(\frac{a(z)}{a(z_L)}\big)^2 + 4\nu\big(\frac{1}{a(z_L)} - \frac{1}{a(z)}\big) = \log\big(\frac{\partial_z\widetilde{\boldsymbol{u}}}{\partial_z\widetilde{\boldsymbol{u}}(z_L)}\big),$$

and replacing their values in the expression provides

$$\log\frac{z_l}{z} + \frac{4\nu}{\widetilde{\kappa}\widetilde{U}_\tau(z_L - z_0)}\big(1 - \frac{\sqrt{z_L}}{\sqrt{z}}\big) = \log\big(\frac{\partial_z\widetilde{\boldsymbol{u}}}{\partial_z\widetilde{\boldsymbol{u}}(z_L)}\big).$$

Therefore the following expression can be obtained, with $C = 4\nu/\big(\widetilde{\kappa}\widetilde{U}_\tau(z_L - z_0)\big)$,

$$\begin{aligned}\widetilde{\boldsymbol{u}}(z) =& \widetilde{\boldsymbol{u}}(z_L) + \partial_z\widetilde{\boldsymbol{u}}(z_L)z_L\exp(C)\int_{z_L}^{z}\frac{1}{z}\cdot\sum_{k=0}^{\infty}\frac{(-C)^k}{k!}\big(\frac{z_L}{z}\big)^{\frac{k}{2}}\mathrm{d}z \\ =& \widetilde{\boldsymbol{u}}(z_L) + \partial_z\widetilde{\boldsymbol{u}}(z_L)z_L\exp(C)\bigg(\log\big(\frac{z}{z_L}\big) + \sum_{k=1}^{\infty}\frac{-2}{k}\frac{(-C)^k}{k!}\bigg(\big(\frac{z_L}{z}\big)^{\frac{k}{2}} - 1\bigg)\bigg). \qquad \text{(A2)}\end{aligned}$$

It can be immediately checked that this profile tends to (24) when the modular viscosity tends to zero.

---

[1] L. Prandtl, "Bericht über untersuchungen zur ausgebildeten turbulenz," Z. Angew. Math. Mech. **5**, 136–139 (1925).

[2] T. von Kármán, "Meckanishe ähnlichkeit und turbulenz," Gött. Nachr. , 58–76 (1930).

[3] J. Jiménez and R. Moser, "What are we learning from simulating wall turbulence?" Phil. Trans. R. Soc. A **365**, 715–732 (2007).

[4] I. Marusic, B. McKeon, P. Monkevitz, H. Nagib A. Smits, and K. Sreenivasan, "Wall-bounded turbulent flows: recent advances and key issues," Phys. Fluids **22** (2010).

[5] J. C. Klewicki, "Reynolds number dependence, scaling, and dynamics of turbulent boundary layers," Trans. ASME J. Fluids Eng. **132**, 1–48 (2010).

[6] I. Marusic, J. Monty, M. Hultmark, and A. Smits, "On the logarithmic region in wall turbulence," J. Fluid Mech. **716**, 1–11 (2013).

[7] M. Reeks, "The transport of discrete particles in inhomogeneous turbulence," J. Aerosol Sci. **14**, 729–739 (1983).

[8] D. Andrews and M. McIntyre, "An exact theory of nonlinear waves on a Lagrangian-mean flow," J. Fluid. Mech. **89**, 609–646 (1978).

[9] E. Mémin, "Fluid flow dynamics under location uncertainty," Geophys. & Astro. Fluid Dyn. **108**, 119–146 (2014).

[10] P. Chandramouli, D. Heitz, S. Laizet, and E. Mémin, "Coarse large-eddy simulations in a transitional wake flow with flow models under location uncertainty," Comp. & Fluids **168**, 170–189 (2018).

[11] S. Kadri Harouna and E. Mémin, "Stochastic representation of the Reynolds transport theorem: revisiting large-scale modeling," Computers & Fluids **156**, 456–469 (2017).

[12] V. Resseguier, E. Mémin, D. Heitz, and B. Chapron, "Stochastic modelling and diffusion modes for proper orthogonal decomposition models and small-scale flow analysis," J. Fluid Mech. **828**, 29 (2017).

[13] G. Da Prato and J. Zabczyk, *Stochastic equations in infinite dimensions* (Cambridge University Press, 1992).

[14] B. Sawford., "Generalized random forcing in random-walk models of turbulent dispersion model," Phys. Fluids **29**, 3582–3585 (1986).

[15] D. Haworth and S. Pope, "A generalized Langevin model for turbulent flows." Phys. Fluids **29**, 387–405 (1986).

[16] S. Pope, "Lagrangian pdf methods for turbulent flows," Annu. Rev. Fluid Mech. (1994).

[17] S. Pope, *Turbulent flows* (Cambridge University Press, 2000).

[18] V. Resseguier, E. Mémin, and B. Chapron, "Geophysical flows under location uncertainty, Part I Random transport and general models," Geophys. & Astro. Fluid Dyn. **111**, 149–176 (2017).

[19] V. Resseguier, E. Mémin, and B. Chapron, "Geophysical flows under location uncertainty, Part II Quasi-geostrophy and efficient ensemble spreading," Geophysical and Astrophysical Fluid Dynamics **111**, 177–208 (2017).

[20] V. Resseguier, E. Mémin, and B. Chapron, "Geophysical flows under location uncertainty,

Part III SQG and frontal dynamics under strong turbulence conditions," Geophysical and Astrophysical Fluid Dynamics **111**, 209–227 (2017).

[21] B. Chapron, P. Dérian, E. Mémin, and V. Resseguier, "Large-scale flows under location uncertainty: a consistent stochastic framework," QJRMS **144**, 251–260 (2018).

[22] D.D. Holm, "Variational principles for stochastic fluid dynamics," Proc. R. Soc. A **471** (2015).

[23] D. Crisan, F. Flandoli, and D.D Holm, "Solution properties of a 3D stochastic Euler fluid equation," J. Nonlinear Sci. , 1–58 (2018).

[24] C.J. Cotter, G.A. Gottwald, and D.D Holm, "Stochastic partial differential equations as a diffusive limit of deterministic Lagrangian multi-time dynamics," Proc. R. Soc. A **473: 20170388** (2017).

[25] M. Caporaloni, F. Tampieri, F. Trombetti, and O. Vittori, "Transfer of particles in non-isotropic air turbulence." J. Atmos. Sci. **32**, 565–568 (1975).

[26] J. Macinnes and F. Bracco, "Stochastic particles dispersion modelling and the tracer-particle limi," Phys. Fluids **4**, 2809–2824 (1992).

[27] J. Jimenez, "Coherent structures in wall-bounded turbulence," J. Fluid. Mech. **842**, 1–100 (2018).

[28] J.A. Sillero, J. Jiménez, and R.D. Moser, "One-point statistics for turbulent wall-bounded flows at Reynolds numbers up to $\delta^+ \approx 2000$," Physics of Fluids **25**, 105102 (2013).

[29] Y. Mizuno M. P. Simens J. Jimenez, S. Hoyas, "A high-resolution code for turbulent boundary layers," Journal of Computational Physics **228**, 4218–4231 (2009).

[30] J. Jimenez G. Borrell, J.A. Sillero, "A code for direct numerical simulation of turbulent boundary layers supercomputers," Computers & Fluids **80**, 37–43 (2013).

[31] G.K. El Khoury, P. Schlatter, A. Noorani, P.F. Fischer, and A. V Brethouwer, G.and Johansson, "Direct numerical simulation of turbulent pipe flow at moderately high Reynolds numbers," Flow, turbulence and combustion **91**, 475–495 (2013).

[32] M. Lee and R.-D. Moser, "Direct numerical simulation of turbulent channel flow up to $\mathrm{Re}_\tau = 5200$," J. Fluid Mech. **774**, 395–415 (2015).

[33] D. B. Spalding, "A single formula for the "law of the wall"," J. of Applied Mech. **28**, 455–458 (1961).

[34] U. Högström, "Review of some basic characteristics of the atmospheric surface layer," Boundary-Layer Meteorol. , 215–246 (1996).